International Journal of Multiphase Flow 35 (2009) 142–154

Contents lists available at ScienceDirect

International Journal of Multiphase Flow

journal homepage: www.elsevier.com/locate/ijmulflow

Effects of heat flux, mass flux, vapor quality, and saturation temperature on flow boiling heat transfer in microchannels

Stefan S. Bertsch [a,b], Eckhard A. Groll [a,b], Suresh V. Garimella [b,*]

[a] Ray W. Herrick Laboratories, School of Mechanical Engineering, Purdue University, 585 Purdue Mall, West Lafayette, IN 47907-2088, USA
[b] Cooling Technologies Research Center, School of Mechanical Engineering, Purdue University, 585 Purdue Mall, West Lafayette, IN 47907-2088, USA

ARTICLE INFO

Article history:
Received 23 July 2008
Accepted 8 October 2008
Available online 1 November 2008

ABSTRACT

Flow boiling heat transfer with the refrigerants R-134a and R-245fa in copper microchannel cold plate evaporators is investigated. Arrays of microchannels of hydraulic diameter 1.09 and 0.54 mm are considered. The aspect ratio of the rectangular cross section of the channels in both test sections is 2.5. The heat transfer coefficient is measured as a function of local thermodynamic vapor quality in the range −0.2 to 0.9, at saturation temperatures ranging from 8 to 30 °C, mass flux from 20 to 350 kg m^{-2} s^{-1}, and heat flux from 0 to 22 W cm^{-2}. The heat transfer coefficient is found to vary significantly with heat flux and vapor quality, but only slightly with saturation pressure and mass flux for the range of values investigated. It was found that nucleate boiling dominates the heat transfer. In addition to discussing measurement results, several flow boiling heat transfer correlations are also assessed for applicability to the present experiments.

1. Introduction

Flow boiling in microchannels has been investigated in recent years due to its capability of handling the high heat fluxes encountered in the cooling of electronic components (Garimella and Sobhan, 2003; Thome, 2004; Garimella et al., 2006). In comparison to cooling solutions with single-phase fluid loops, flow boiling provides higher heat transfer coefficients at lower mass flow rates, and results in a more even surface temperature distribution due to the constant fluid temperature in the two-phase regime (Hetsroni et al., 2004). Trutassanawin et al. (2006) and Mongia et al. (2006) showed that vapor compression systems are a viable alternative to constant-pressure fluid loops due to the possibility of reducing the coolant temperature below ambient temperature conditions.

An understanding of the fundamental heat transfer processes in the cold plate evaporator is necessary in such applications to predict the heat transfer performance and pressure drop and optimize the design. Although many studies (Chang and Pan, 2007; Chen and Garimella, 2006; Harirchian and Garimella, 2008; Lee and Garimella, 2007; Liu et al., 2005; Qu and Mudawar, 2004; Steinke and Kandlikar, 2004, and Wu and Cheng, 2003) have addressed this topic, flow boiling in microchannels has not yet been fully understood.

A number of reviews of the literature on this topic have been published, such as those by Bertsch et al. (2008b), Dupont and Thome (2005), Kandlikar et al. (2003), Vlasie et al. (2004). While there has been general agreement in the published results that the heat transfer coefficient increases with increasing heat flux, the effect of several other parameters such as vapor quality and mass flux have received less attention and shown opposing trends in the literature in some cases. For example, Bao et al. (2000) and Lazarek and Black (1982) reported an almost constant heat transfer coefficient with respect to thermodynamic vapor quality for flow boiling in microchannels. On the other hand, Saitoh et al. (2005) found a significant increase in heat transfer coefficient at high vapor qualities, as is typically observed in conventional-sized channels. Bertsch et al. (2008a), Yan and Lin (1998), Yun et al. (2006), and Lin et al. (2001) found a peak in the heat transfer coefficient for vapor qualities between 0.1 and 0.6 followed by a drop-off at higher vapor qualities.

In view of some of these contradictory results in the literature, the local flow boiling heat transfer coefficient of two different refrigerants in microchannels is investigated in the present study through well-characterized experiments as a function of heat flux, mass flux, vapor quality, saturation pressure and channel size. An earlier study by Bertsch et al. (2008a) discussed a new test setup that was developed for these experiments along with experimental results for the refrigerant R-134a in channels with a hydraulic diameter of 1.09 mm. The present work significantly expands the measurement database by considering smaller channels as well as a second fluid, and discusses the influence of several parameters such as heat flux, mass flux, vapor quality, and channel hydraulic diameter. In addition, the measurements are compared to predictions from a wide range of correlations in the literature.

The bulk of the experiments are carried out with refrigerant R-134a since it is one of the most suitable choices for microelectronics thermal management applications as pointed out by

* Corresponding author. Tel.: +1 765 494 5621.
E-mail address: sureshg@purdue.edu (S.V. Garimella).

0301-9322/$ - see front matter © 2008 Elsevier Ltd. All rights reserved.
doi:10.1016/j.ijmultiphaseflow.2008.10.004

Trutassanawin et al. (2006) and Mongia et al. (2006). The second refrigerant, R-245fa, was chosen due to its advantages of a low saturation pressure at ambient temperature conditions, a low freezing point, non-flammable nature, and its good materials compatibility. From an environmental perspective, neither fluid has an Ozone Depletion Potential (ODP), but the Global Warming Potential (GWP) of R-245fa is almost six times as high as that of R-134a (Calm and Hourahan, 2001). But the low saturation pressure of R-245fa compared to other refrigerants could result in lighter equipment and easier servicing. Only a few studies to date have investigated the thermal characteristics of R-245fa (Revellin and Thome, 2007 and Kedzierski, 2006).

It is noted that the primary objective of the experiments in this work is to obtain the heat transfer coefficient during flow boiling of refrigerants through multiple parallel microchannels as a function of refrigerant quality. The width of the microchannels and the intervening fins are not optimized to maximize the total heat transfer rate from the cold plate.

2. Experimental setup and data reduction

The experimental facility and procedures used in this work are the same as those described in Bertsch et al. (2008a). An abbreviated description is included here for completeness.

Fig. 1 shows the measurement plan of the test setup used to investigate the heat transfer during refrigerant flow boiling in microchannels. Locations of the different sensors are indicated in the schematic as are some state points (number 1 through 6) which will be used in the discussion here. The setup consists of a hermetically sealed fluid loop with a variable-speed gear pump which obviates the use of lubricants, a 7-μm filter, the test section, a condenser, several valves to regulate the flow, and instrumentation. Refrigerant pressure in the setup is adjusted using an accumulator with a membrane that is pressurized with nitrogen. The condenser and subcooler are cooled by a constant temperature bath which is capable of achieving temperatures from −20 to +30 °C. The state points in this figure are shown on a pressure-enthalpy diagram in Bertsch et al. (2008a). In general, subcooled liquid (vapor quality between −0.25 and −0.1) enters the test section assembly which consists of several heated and adiabatic sections.

The term test section assembly refers to the component shown in the detailed drawing in Fig. 2a. The test section assembly contains the pre-evaporator, test piece, post-evaporator, adiabatic sections, inlet and outlet manifold, and the housing. Compared to the test section assembly described in Bertsch et al. (2008a), the durability of the housing was improved in the present work by adding two stainless steel plates containing all the fittings. These two stainless steel plates were attached to the top piece using face seals to reduce mechanical stress on the polycarbonate housing. Fig. 2b shows a photograph of the assembly. The inner part of the test section assembly, without the housing, is referred to as the test section, and contains seven elements in the following order in the flow direction: Inlet manifold, pre-evaporator, adiabatic section, test piece, adiabatic section, post-evaporator, and outlet manifold. The test piece is the single heated copper block in the middle of the test section, on which most of the actual measurements and analysis are performed.

The refrigerant evaporates in the pre-evaporator from state point 3 to 4, which provides the desired inlet quality for the test piece. The actual test piece is located between state points 4 and 5, where the local heat transfer coefficient is measured. After leaving the test piece, the refrigerant is heated to state point 6 in the post-evaporator so that the refrigerant reaches a superheated state. The refrigerant is then cooled back to state point 1 in the liquid-cooled condenser. Three independent sets of cartridge heaters with adjustable input power are used in the pre-evaporator, test piece and post-evaporator to provide heat input. This setup thus allows for easy and independent adjustment of the inlet and outlet vapor quality, mass flux, heat flux and saturation pressure. It also leads to determination of the heat flux and vapor quality by multiple, redundant approaches.

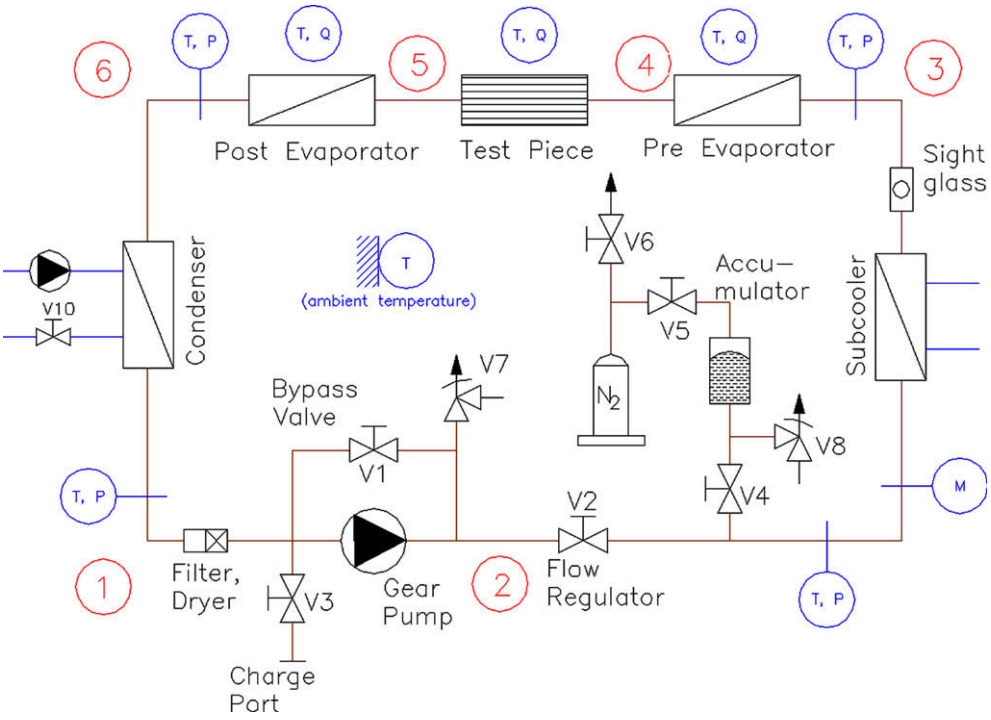

Fig. 1. Measurement plan for the vapor quality-based investigation of flow boiling in microchannels.

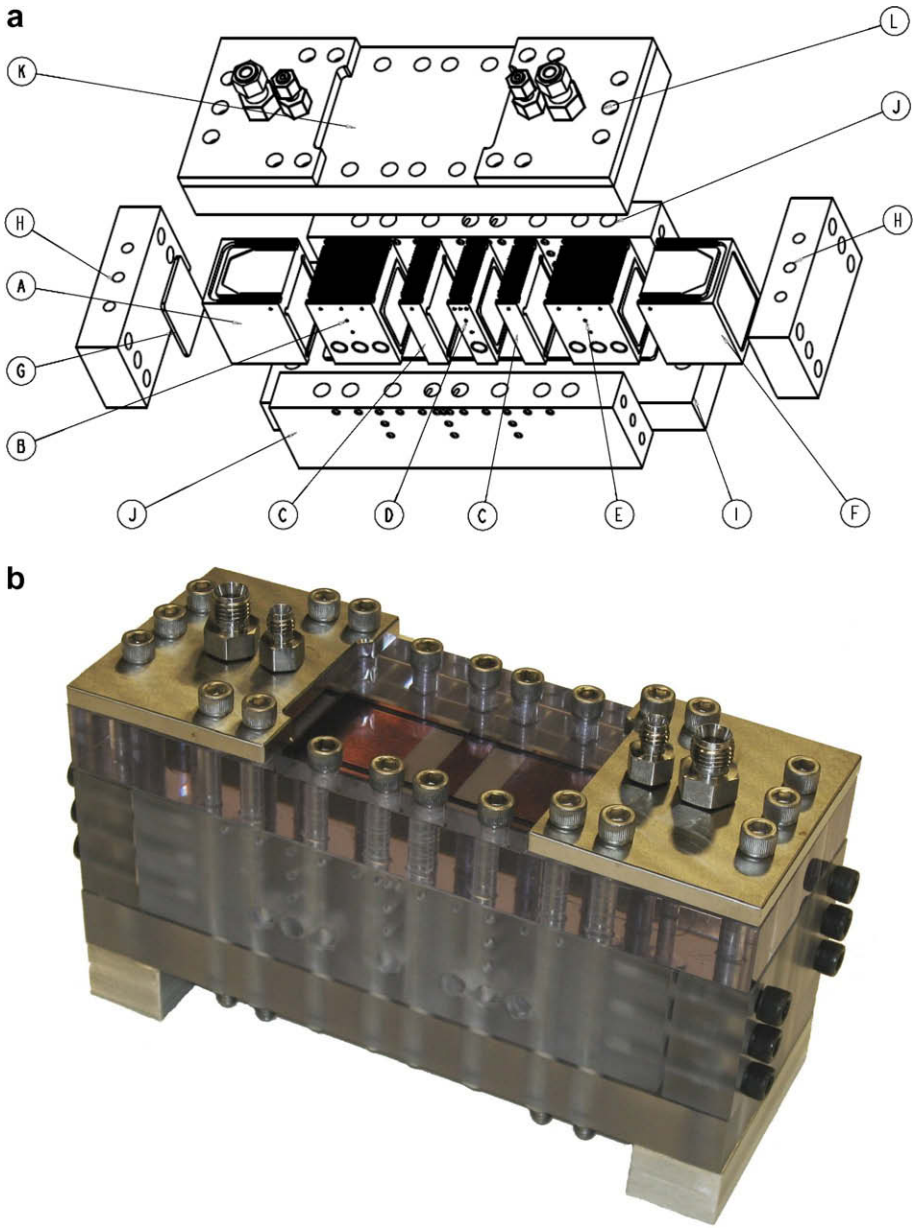

Fig. 2. Test section assembly: (a) exploded view with the components (A) inlet piece, (B) pre-evaporator, (C) adiabatic piece, (D) test piece, (E) post-evaporator, (F) outlet piece, (G) rubber compression, (H) front and back pieces, (I) bottom piece, (J) side pieces, (K) top piece and (L) stainless steel plate with fluid ports, and (b) photograph of the assembly.

Adiabatic sections located between the three heated blocks are made of a thermoplastic (PEEK) which has a low thermal conductivity (0.25 $W\,m^{-1}\,K^{-1}$), and has good chemical resistance to the working fluids. The heated blocks (pre-evaporator, test piece and post-evaporator) are made of oxygen-free copper and contain the cartridge heaters and several thermocouples. A thin silicone sheet on top of the microchannels prevents cross leakage from one channel into the next. The cover plate is made of polycarbonate and allows optical access to the test section from the top. The assembly is compressed with rubber sheets on the side and bottom (part G in Fig. 2, top) to allow for thermal expansion and is well insulated to prevent heat losses to ambient. Exact alignment of the microchannels in successive sections of the assembly was achieved using small gaps and recesses between the heated and adiabatic sections.

Table 1 lists the important dimensions of the two different microchannel test pieces together with the measurement and fabrication uncertainties. Test section #1 contains 17 rectangular channels with a height-to-depth ratio of 2.5 and a hydraulic diameter of 1.08 mm. Test section #2 contains 33 channels with a hydraulic diameter of 0.54 mm and the same aspect ratio as test section #1. Before charging the setup, the system was always evacuated and the refrigerant filter-dryer was replaced in between the measurements with the fluids R-134a and R-245fa.

Calibrated T-type thermocouples with a maximum error of ±0.5 °C were used to measure temperatures in the test section and in the flow stream. Additional details about the exact positioning of the thermocouples and the extrapolation used to determine the surface temperature can be found in Bertsch et al. (2008a).

The electrical power to the DC cartridge heaters was calculated using voltage and current measurements from a shunt resistor, which leads to an uncertainty of 1.5%. The refrigerant mass flow rate was measured using a Coriolis-type mass flow meter with

Table 1
Dimensional details of the microchannel test sections.

Dimension	Test section #1	Test section #2
Number of channels	17	33
Hydraulic diameter, μm	1089 ± 2.6	544 ± 2.3
Channel depth, μm	1905 ± 10	953 ± 10
Fin width, μm	762 ± 2	381 ± 2
Channel width, μm	762 ± 2	381 ± 2
Aspect ratio (depth/width)	2.5	2.5
Length (Test piece), mm	9.53 ± 0.02	9.53 ± 0.02
Length (Pre-evaporator), mm	30.16 ± 0.02	30.16 ± 0.02
Length (Post-evaporator), mm	30.16 ± 0.02	30.16 ± 0.02
Length (adiabatic sections), mm	9.53 ± 0.02	9.53 ± 0.02
Roughness copper, μm	<0.6	<0.5
Roughness (adiabatic sections), μm	<0.7	<0.8
Misalignment, μm	<2.0	<2.0

an uncertainty of 0.2% of the reading within the measurement range. Pressures at three different points in the setup were measured using absolute pressure transducers with a range of 1700 kPa and an accuracy of 0.25% of full scale when using the refrigerant R-134a. For the low pressure refrigerant R-245fa, absolute pressure sensors with a range of 340 kPa and an accuracy of 0.5% of full scale were used. The differential pressure measurement over the test section was measured using a transducer with a range of 70 kPa and an uncertainty of 0.1% of full scale. Each reported measurement was obtained as an average of approximately 45 data points obtained over several minutes of steady-state data. A standard error analysis (Taylor, 1997) was used to estimate the uncertainties in the reported results. The average and maximum uncertainty in the local heat transfer measurements was 7.9% and 11.8%, respectively, for R-134a, with the lowest uncertainty being achieved under subcooled conditions and the highest at low flow rates and low heat fluxes in the saturated flow boiling regime. The corresponding uncertainties in the heat transfer coefficient for the fluid R-245fa were 5.8% and 11.4%.

The average and maximum uncertainties in the vapor quality were 1.2% and 2.1%, respectively. The average and maximum uncertainties in the heat flux calculations were 2.8% and 3.0%, respectively. In addition to the instrumentation discussed above, a camcorder was positioned above the test section assembly to visually observe the flow.

All data reduction procedures were programmed with the Engineering Equation Solver EES software (Klein, 1992–2007). In order to quantify the refrigerant qualities at the different state points, the equations listed below were used. The enthalpy at the inlet (i_3) of the test section assembly is defined by the pressure (P) and temperature (T) knowing that the inlet state is in the subcooled single-phase regime. Knowing the enthalpy of the saturated liquid ($i_{f,sat}$) and the enthalpy of vaporization (i_{fg}) the thermodynamic vapor quality x_3 at the inlet of the test section can be defined as

$$x_3 = \frac{i_3 - i_{f,sat}}{i_{fg}}. \tag{1}$$

From the know inlet condition, the vapor quality at all other state points can be calculated using the measured heat addition and assuming no heat losses in the test section with

$$x = x_3 + \frac{\dot{Q}}{\dot{m} \cdot i_{fg}} \tag{2}$$

where $\dot{m}$ is the refrigerant mass flow rate and $\dot{Q}$ is the sum of the electrical heat input for the respective heated blocks.

The heat transfer coefficient is then defined as

$$H = \frac{q''}{T_{surff} - T_{fl}} \tag{3}$$

where the wall heat flux is defined for the heated wetted area as

$$q'' = \frac{\dot{Q}}{N \cdot L \cdot (W + 2 \cdot H)} \tag{4}$$

and N is the number of channels, L is the length of the heated block, and W and H are the width and height of a microchannel, respectively.

As explained in Bertsch et al. (2008a), the surface temperature (T_{surf}) along the flow direction is assumed constant due to the short length of the test piece; the temperature along the fins was assumed constant due to high values of fin efficiency from 96.5% to 99.9%. The temperature variations in the test piece in the lateral direction were determined using steady-state thermal simulations and showed a maximum lateral variation in the wall temperature over all the interior channels of 0.3 °C.

Since the refrigerant enters the test piece in some cases as subcooled liquid, the length of the channel can be divided into two regions: the upstream subcooled region and the downstream saturated region. Therefore, the temperature difference between fluid and heated surface was calculated on each heated block as follows:

$$T_{surf} - T_{fl} = \frac{L_{sub} \cdot \Delta T_{LMTD} + (L_{tot} - L_{sub}) \cdot (T_{surf} - T_{sat})}{L_{tot}} \tag{5}$$

where L_{sub} is the length of the channel exposed to subcooled liquid, L_{tot} is the entire length of the heated block, and T_{sat} is the saturation temperature of the liquid. Due to the assumption of an isothermal heated surface in flow direction, a log mean temperature difference approach was used to estimate the temperature difference in the subcooled section

$$\Delta T_{LMTD} = \frac{(T_{surf} - T_{sat}) - (T_{surf} - T_{in})}{\ln\left(\frac{T_{surf} - T_{sat}}{T_{surf} - T_{in}}\right)} \tag{6}$$

with T_{in} being the fluid temperature at the inlet of the microchannels.

If the fluid enters the heated block at saturation conditions, Eqs. (5) and (6) reduce to

$$T_{surf} - T_{fl} = T_{surf} - T_{sat}. \tag{7}$$

The pressure drop across the test section assembly consisting of the pre-evaporator, test piece and post-evaporator was assumed linear for the calculation of the saturation temperature T_{sat}. More information on data evaluation and data reduction can be found in Bertsch et al. (2008a).

3. Experimental results

3.1. Energy balance

To establish confidence in the experimentally determined heat transfer coefficients with the given test setup, the energy balance obtained across the test section assembly was first evaluated for single-phase fluid flow. Single-phase flow was chosen since the state points at the inlet and outlet of the test piece are easily defined from known temperatures and pressures in this case. Using these state points and the refrigerant mass flow rate, the heat flux can be calculated as follows:

$$q''_{heatbalance} = \frac{\dot{m} \cdot (i_6 - i_3)}{A_{surf}} \tag{8}$$

where A_{surf} is the heated, wetted surface area of the heated block.

The heat flux determined through the energy balance was then compared to the heat flux obtained through a conduction analysis. The known thermal conductivity and dimensions of the heated copper block together with the temperature gradient in the heat

flow direction measured with four thermocouples was used to determine this heat flux $q''_{conduction}$.

Finally, the heat fluxes obtained through the energy balance and the conduction analysis above were compared to the heat flux calculated from the measured electrical heat input $\dot{Q}_{electric}$ and the known geometry

$$q''_{electric} = \frac{\dot{Q}_{electric}}{A_{surf}} \quad (9)$$

Fig. 3 shows the results of the energy balance calculations for the refrigerant R-245fa in test section #2. As can be seen in Fig. 3, the maximum deviation between the three approaches is 0.68 W cm^{-2}, while the average absolute deviation is 0.39 W cm^{-2}. Therefore, the maximum uncertainty in heat flux is 3.2%, while the average is 1.9% of the maximum heat flux encountered. The energy balance measurements for R-134a in test section #1 showed a maximum error of 0.83 W cm^{-2} and an average error of 0.37 W cm^{-2}. The respective values for R-134a with test section #2 were 0.64 and 0.28 W cm^{-2}. The three different methods of determining heat flux lead to results that cannot be distinguished within the uncertainties, pointing to the robustness of the experimental design, instrumentation, and measurement accuracy. Due to the excellent energy balance, heat losses are neglected in this study.

3.2. Single-phase measurements

Single-phase heat transfer measurements were carried out to further evaluate the capabilities and measurement uncertainty of the test setup. The measurement results were then compared to predictions from the Hausen (1943) and Sieder and Tate (1936) correlations. These correlations were established for developing flow at low Reynolds numbers and a constant surface temperature boundary condition. The measured single-phase liquid heat transfer coefficients with test section #2 are shown in Fig. 4 as a function of Reynolds number for both refrigerants. The saturation pressures at the exit of the test section for R-245fa and R-134a were 145 and 630 kPa, respectively, corresponding to saturation temperatures of 24.2 and 23.2 °C, respectively. It can be seen that the heat transfer coefficient for R-245fa in single-phase flow is higher than that for R-134a due to the difference in thermophysical properties as listed in Table 2.

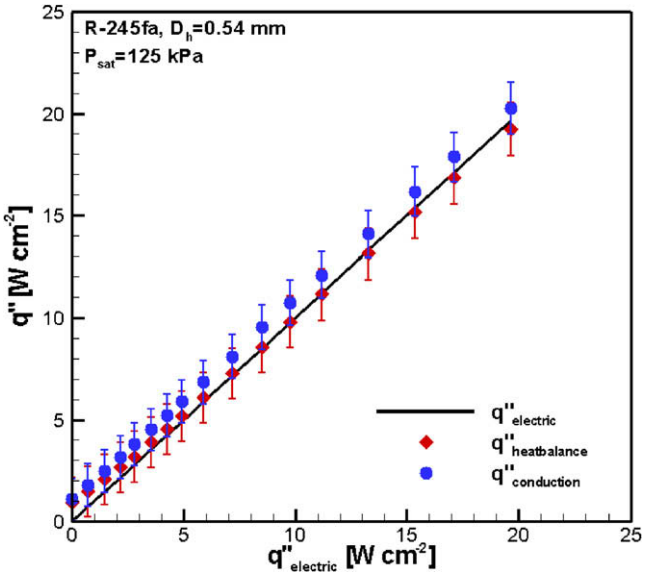

Fig. 3. Energy balance of the setup for refrigerant R-245fa with test section #2.

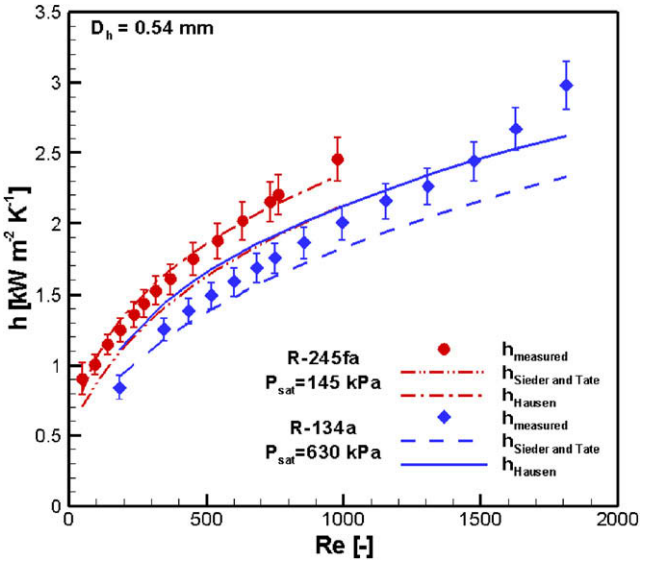

Fig. 4. Measured single-phase heat transfer coefficient for R-134a and R-245fa compared to predictions for developing flow from Hausen (1943) and Sieder and Tate (1936).

Table 2
Thermodynamic properties of the fluids R-134a and R-245fa (Refprop7, 2002).

Property	R-134a	R-245fa
Critical pressure, kPa	4067	3640
Critical temperature, °C	101.1	154.1
Molecular mass, kg kmol^{-1}	102.0	134.1
Saturation pressure (@ 20 °C), kPa	571.6	124.0
Prandtl number (@ 20 °C)	2.74	6.27
Surface tension (@ 20 °C), N m^{-1}	0.0052	0.0147
Density (liquid @ 20 °C), kg m^{-3}	1225.3	1352.0
Density (vapor @ 20 °C), kg m^{-3}	27.8	7.16
Enthalpy of vaporization (@ 20 °C), kJ kg^{-1}	182.3	193.8
Saturation temperature (@ 100 kPa), °C	−26.1	14.9

It can be seen in Fig. 4 that the measured heat transfer coefficients for both fluids fall in between the respective prediction results from the two correlations, and are somewhat closer to the predictions from the Hausen (1943) correlation, which is based on fully developed flow with a thermal entry length and resembles conditions in the current setup. The conclusions from several past studies (e.g., Sobhan and Garimella, 2001 and Lee et al., 2005) that single-phase heat transfer in microchannels can be predicted well with appropriate correlations developed for conventional-sized channels hold true for the present results as well.

3.3. Boiling curve

Boiling curves are plotted for both refrigerants with test section #2 in terms of the variation of wall heat flux with the temperature difference between the wall and saturation temperature as shown in Fig. 5. The results are obtained at six different mass fluxes in the range of 42–334 kg m^{-2} s^{-1} for heat fluxes from 0 to 20 W cm^{-2}. In the case of R-134a (Fig. 5a), the inlet vapor quality was held constant at approximately −0.2 and the saturation pressure at 750 kPa corresponding to a saturation temperature of 29.1 °C. For R-245fa (Fig. 5b), the inlet vapor quality was held constant at approximately −0.1 and the saturation pressure at 155 kPa corresponding to a saturation temperature of 26.0 °C.

It is observed from Fig. 5 that in the single-phase region, the higher mass flow rate supports a higher heat flux at a given wall

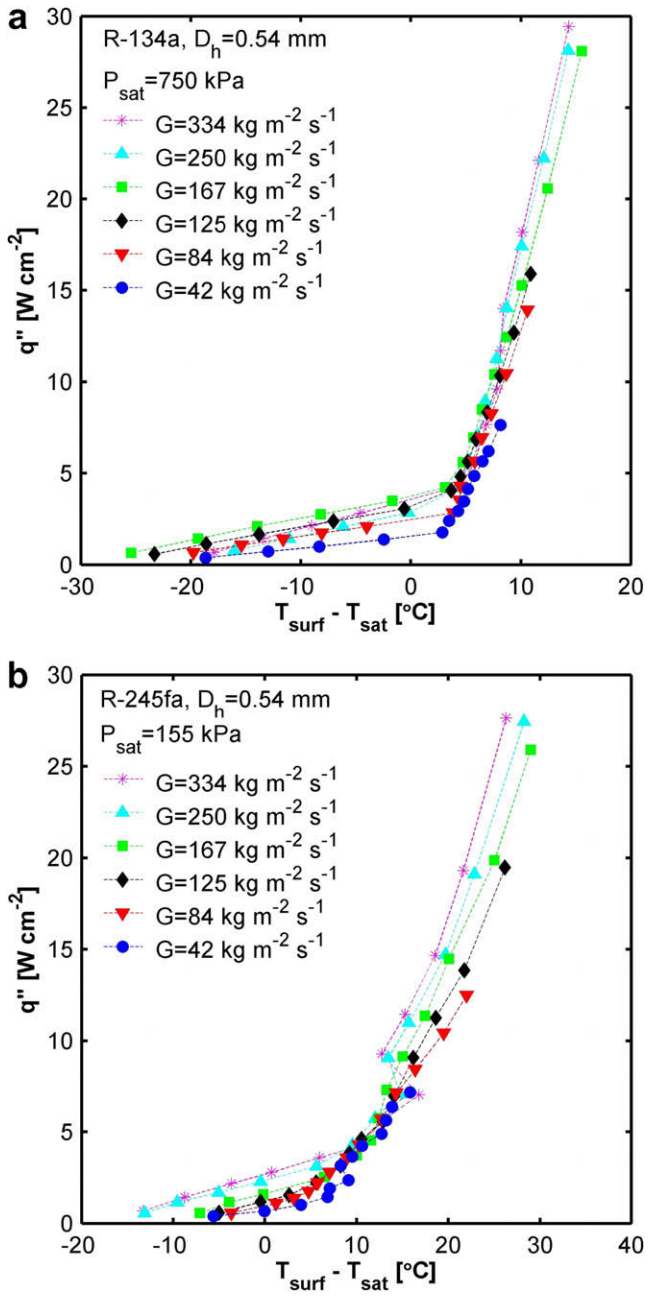

Fig. 5. Boiling curve for (a) R-134a, and (b) R-245fa measured with test section #2.

superheat. In the case of R-134a, no temperature overshoot was observed at the onset of nucleate boiling (ONB). The small overshoot observed with R-245fa may be related to its different wetting behavior. In the case of R-245fa, stable flow regimes were visually observed with nucleate boiling in some of the microchannels while other channels were still in single-phase flow. In contrast, for the measurements using R-134a, the initiation of nucleate boiling in any channel was followed immediately by the establishment of nucleate boiling in all the channels. Due to the higher single-phase heat transfer (see Section 3.2) and lower boiling heat transfer (to be discussed in Section 3.4) observed with R-245fa, the increase in heat transfer after the onset of boiling is less pronounced with this refrigerant. After the onset of nucleate boiling, the boiling curves almost collapse on to a single curve for both fluids irrespective of the inlet temperature and mass flow rate, with a higher mass flux leading to a marginal increase in heat transfer coefficient in both cases. This observation may support the dominance of nucleate boiling over convective heat transfer, which was also found in other past studies such as those of Harirchian and Garimella (2008) and Chen and Garimella (2006). In addition, the onset of nucleate boiling strongly depends on the mass flux, with a higher heat flux observed at ONB with increasing mass flux for both fluids. The critical heat flux (CHF) also increases with mass flux.

The flow patterns visually observed after the onset of boiling revealed a mostly bubbly flow regime, which sometimes transitioned to slug flow at the highest measured heat fluxes. Only at the highest heat flux considered, the onset of high frequency out-of-phase flow instabilities (fluid in adjacent channels oscillates in opposing directions) as described by Tadrist (2007) were observed. Flow instabilities were more prominent at low mass fluxes compared to high mass fluxes. As mentioned before in the case of R-245fa, partial boiling in some of the microchannels and single-phase flow in others could be observed close to the onset of nucleate boiling.

3.4. Heat transfer coefficient as a function of vapor quality

Fig. 6 shows the heat transfer coefficient as a function of thermodynamic vapor quality for R-134a and R-245fa measured with test section #2. In the case of R-134a the saturation pressure was kept constant at 550 kPa corresponding to a saturation temperature of 18.7 °C, while for R-245fa, the respective values were 125 kPa and 20.3 °C. Each point in Fig. 6 represents the heat transfer coefficient measured for a vapor quality change of 0.2 (±0.01) across the test piece. For instance, a point shown as being at a quality of 0.3 implies the average heat transfer coefficient over the thermodynamic quality range from 0.2 to 0.4. The differential of 0.2 in vapor quality across the test piece was chosen as a compromise between measurement uncertainty and resolution. Due to the fixed quality change, mass flux and heat flux are coupled and displayed for all data points. In both measurements, the mass flux and heat flux were varied in six steps from 42 to 334 kg m^{-2} s^{-1} and 2.6–19.6 W cm^{-2}, respectively.

The heat transfer coefficient is seen to increase with increasing heat flux as expected. An increasing heat flux also results in an increasing mass flux, due to the operating conditions discussed above. In both cases the heat transfer coefficient increases strongly up till a vapor quality of 0.1. At low heat and mass fluxes, the heat transfer coefficient for R-134a then stays almost constant up to a vapor quality of 0.5 before it starts to drop-off more rapidly towards higher vapor qualities. At higher heat and mass fluxes, the heat transfer coefficient does not exhibit a plateau, and instead starts decreasing immediately after the initial ascent at low vapor qualities. For R-245fa a very similar trend can be seen, with the difference being that the highest heat transfer coefficient is encountered at vapor qualities of approximately 0.5 with this fluid. In comparison, the measurements on test section #1, described in detail in Bertsch et al. (2008a), showed a peak in heat transfer coefficient for low mass fluxes and similar heat fluxes at a vapor quality of approximately 0.2. Saitoh et al. (2005) found a similar shift in the peak heat transfer coefficient for their studies on microchannels with different dimensions.

As can be seen from a comparison of the two plots in Fig. 6, the heat transfer coefficient during flow boiling of R-245fa is far lower than that for R-134a under the same conditions. The thermodynamic fluid properties shown in Table 2 reveal that the molecular mass (M) of R-245fa is larger than that of R-134a and that its surface tension is higher. An inspection of the Cooper (1984) correlation shows that the pool boiling heat transfer coefficient is proportional to M^{-n}. Further, the pool boiling equation of Bennett and Chen (1980) shows that the heat transfer coefficient is inversely proportional to the surface tension. The measurements in the present work are therefore consistent with the expected trends.

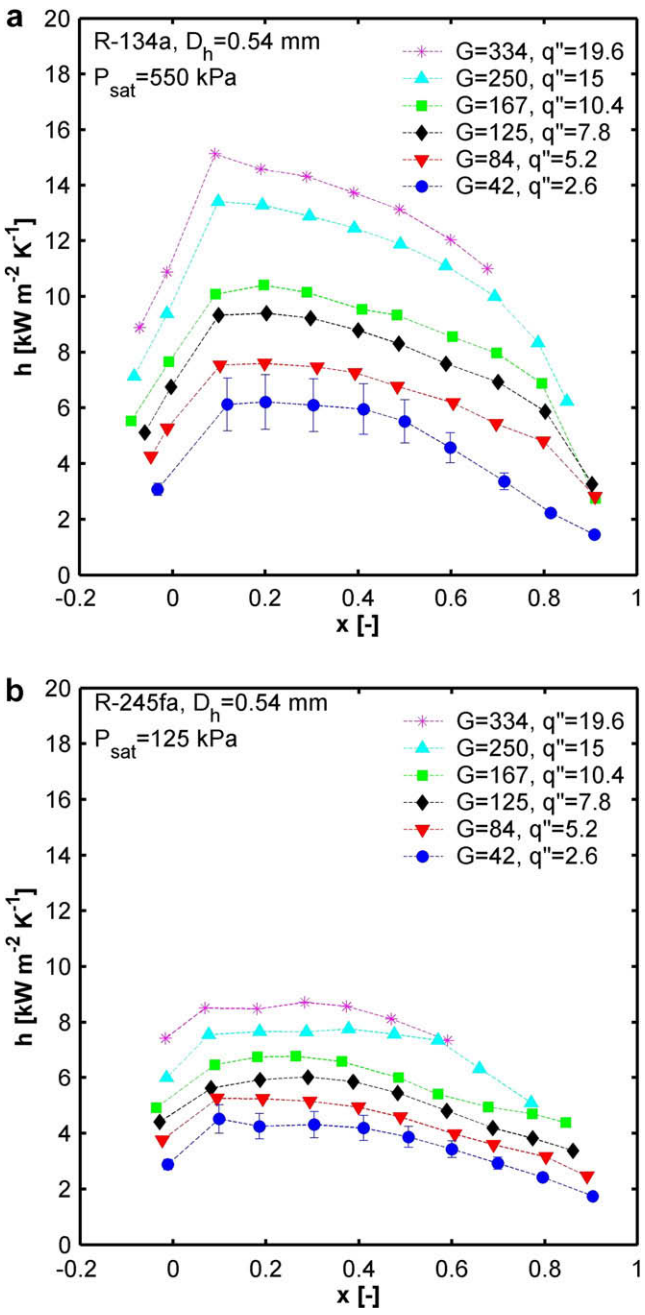

Fig. 6. Effect of thermodynamic vapor quality on the heat transfer coefficient for (a) R-134a, and (b) R-245fa; G in kg m^{-2} s^{-1} and q'' in W cm^{-2}.

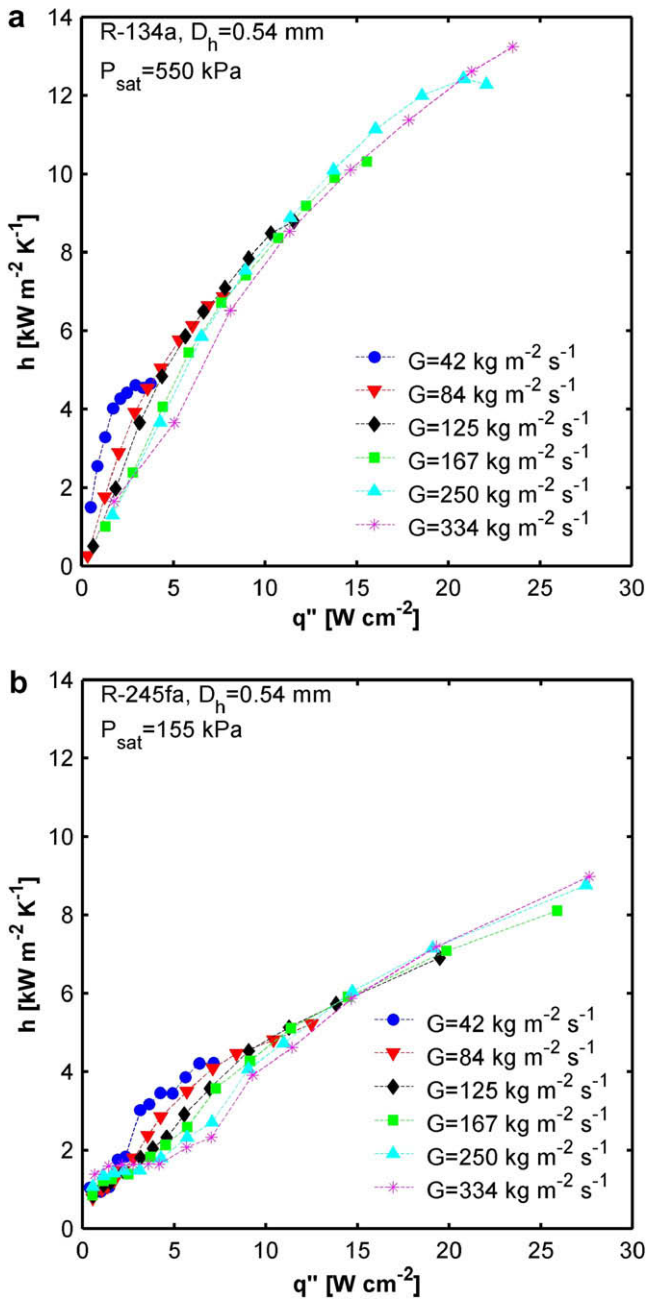

Fig. 7. Effect of heat flux and mass flux on the heat transfer coefficient for (a) R-134a, and (b) R-245fa measured with test section #2.

While the single-phase heat transfer coefficient is higher for R-245fa than for R-134a, the pool boiling heat transfer coefficient is higher for R-134a. Since the flow boiling heat transfer coefficient for R-245fa is smaller than for R-134a, this again indicates that nucleate boiling dominates the heat transfer in microchannels in the investigated range of mass fluxes.

Visual observation revealed that for most of the measurements presented in this work of heat transfer versus vapor quality, the flow regimes could best be described as slug or intermittent flow. Out-of-phase flow instabilities were restricted to low mass fluxes.

3.5. Heat transfer coefficient as a function of heat flux

The effect of heat flux on the average heat transfer coefficient for R-134a and R-245fa is illustrated in Fig. 7. Tests were conducted on test section #2 for six different mass fluxes ranging from 42 to 334 kg m^{-2} s^{-1}. The saturation pressure of R-134a at the outlet of the test section was held constant at 550 kPa corresponding to a saturation temperature of 18.7 °C; the corresponding values for R-245fa were 155 kPa and 20.0 °C. The vapor quality at the inlet for R-134a was approximately −0.2 for the experiments and −0.1 for R-245fa.

It can be seen from Fig. 7 that the heat transfer coefficient steadily increases with increasing heat flux. At very low heat fluxes, and again at high-heat fluxes beyond 10 W cm^{-2}, the heat transfer coefficients for all mass fluxes collapse to a single set of curves in both plots. Only in the region from 2 to 10 W cm^{-2} does the mass flux show a significant effect on the heat transfer coefficient. A similar trend was also found by Harirchian and Garimella (2008) for the dielectric liquid, FC-77. The lowest mass flux leads to the

highest value of heat transfer coefficient for both fluids. This apparently surprising result can be explained in view of the fact that at a given heat flux, the vapor quality at the outlet is higher for a lower mass flux. The heat transfer coefficient increases significantly during the transition from the single-phase to the two-phase flow regime with an increase in heat flux, which occurs earlier for a lower mass flux. The influence of vapor quality on heat transfer coefficient outweighs the mass flux effect. When plotting the same results versus vapor quality instead of heat flux, the behavior presented in Section 3.4 is observed. Therefore, great care should be taken when interpreting the trends of variation of the heat transfer coefficient with different parameters.

3.6. Heat transfer coefficient as a function of saturation pressure (temperature)

The effect of saturation pressure on the local heat transfer coefficient for R-134 in test section #2 is illustrated in Fig. 8. At a fixed heat flux and mass flux of 167 kg m^{-2} s^{-1} and 10.4 W cm^{-2}, respectively, three different values of saturation pressure were tested – 400, 550, and 750 kPa, corresponding to saturation temperatures of 8.9, 18.7 and 29.1 °C. Each point in Fig. 8 represents the heat transfer coefficient measured for a vapor quality change of 0.2 (±0.01) across the test piece as discussed earlier. Even though the measurements cannot be distinguished within the measurement uncertainty, it appears that an increase in saturation pressure leads to a slight increase in heat transfer coefficient. Similar results were reported by Saitoh et al. (2005).

3.7. Heat transfer coefficient as a function of hydraulic diameter

Fig. 9 shows the heat transfer coefficient as a function of the thermodynamic vapor quality for two different hydraulic diameters, 1.09 mm (test section #1) and 0.54 mm (test section #2). The measurements were conducted for R-134a at a saturation pressure of 550 kPa, which corresponds to a saturation temperature of 18.7 °C. Due to the different cross-sectional areas of the two flow channels, a quality change of 0.2 at a certain heat flux leads to a higher mass flux in test section #2.

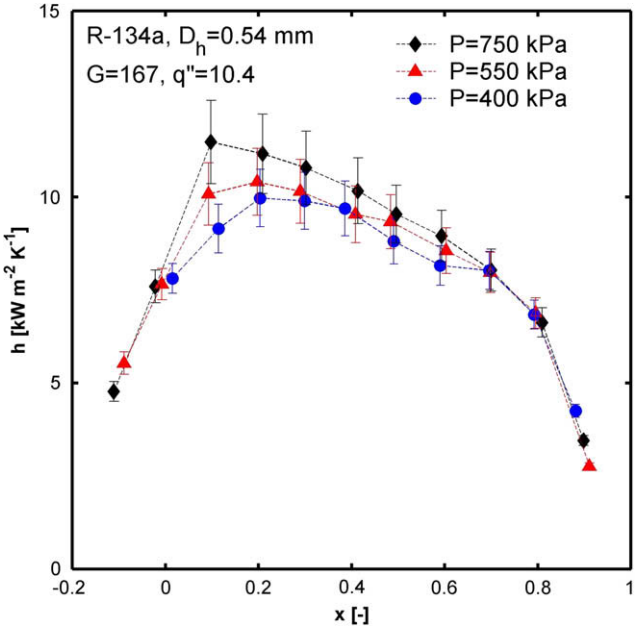

Fig. 8. Effect of saturation pressure on the heat transfer coefficient for R-134a; G in kg m^{-2} s^{-1} and q'' in W cm^{-2}.

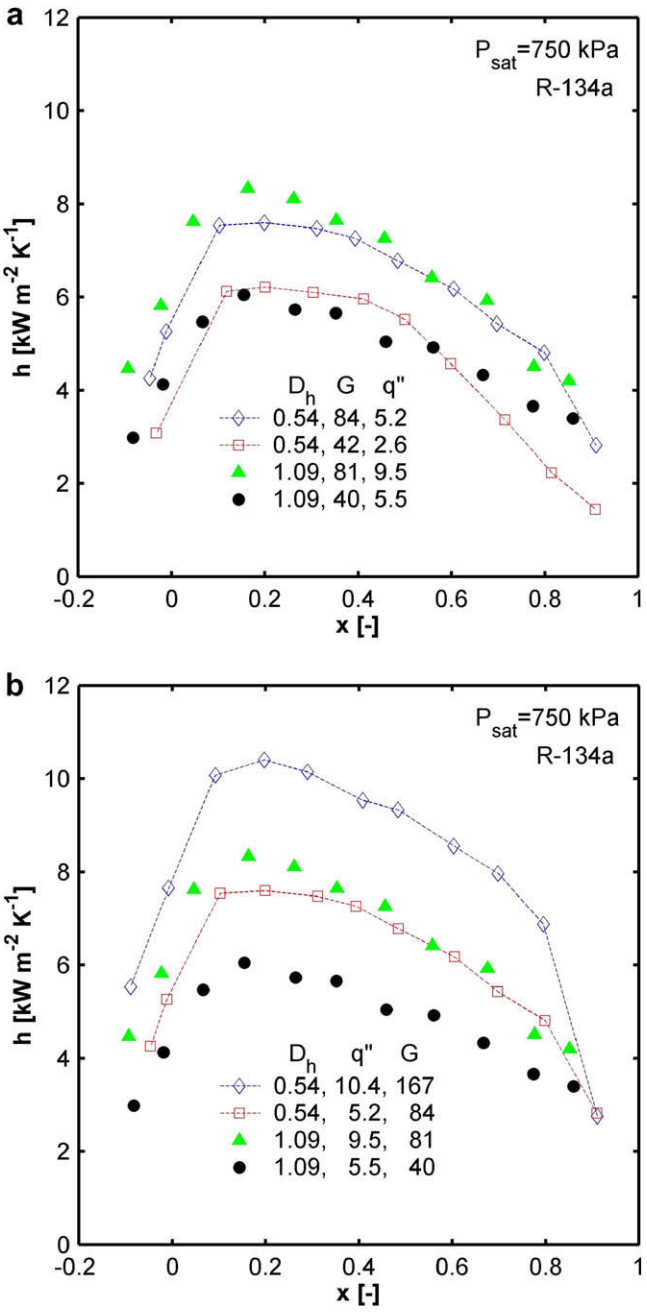

Fig. 9. Effect of hydraulic diameter on the heat transfer coefficient for R-134a; D_h in mm, q'' in W cm^{-2} and G in kg m^{-2} s^{-1}. Part (a) shows results with two similar mass flux ranges and part (b) two similar heat fluxes.

In Fig. 9a, the mass flux between the two geometries was held at similar levels. It can be seen that the heat transfer coefficients for both microchannel diameters show similar values. However, the heat flux for the 1.09 mm channels is twice as high at the same mass flux compared to the 0.54 mm channels. In Fig. 9b the heat flux between the two geometries was held at similar levels. This time the heat transfer coefficient of the smaller channels is higher at similar heat fluxes. In this case, the mass flux is higher for the smaller channels.

A comparison of the two plots indicates that the heat transfer coefficient for the smaller hydraulic-diameter channels is slightly higher than for the larger channels. However, this effect is small compared to the effects of heat flux and vapor quality. A detailed study of the influence of channel dimensions on heat transfer

Table 3
Studies in the literature from which flow boiling heat transfer correlations are selected, and their ranges of applicability.

Author(s)	Fluid, channel geometry	Parameter range
Bennett and Chen (1980)	Water, methanol, pentane, heptane, benzene, ...	P = 55 kPa–3.5 Mpa q'' = 0.6–240 W cm^{-2} x = 0.01–0.71
Lazarek and Black (1982)	R-113 D_h = 3.1 mm	G = 125–750 kg m^{-2} s^{-1} q'' = 1.4–38 W cm^{-2} x = 0.0–0.6
Shah (1982)	Several refrigerants D_h = 5.0–15.8 mm	G = 70–11071 kg m^{-2} s^{-1} q'' = 9–121.5 W cm^{-2} x = 0.0–0.7
Liu and Winterton (1991)	Water and refrigerants D_h = 2.95–32.0 mm	G = 12.4-8157 kg m^{-2} s^{-1} q'' = 0.35−262 W cm^{-2} x = 0.0–0.95
Tran et al. (1996)	R-12, R-113 D_h = 2.4–2.92 mm	G = 44–832 kg m^{-2} s^{-1} q'' = 0.36–12.9 W cm^{-2} P = 510–820 kPa x = 0–0.94
Lee and Lee (2001)	R-113 D_h = 0.78-3.6 mm	G = 50–200 kg m^{-2} s^{-1} q'' = 0–1.5 W cm^{-2} x = 0.15–0.75
Warrier et al. (2002)	FC-84 D_h = 0.75 mm	G = 557–1600 kg m^{-2} s^{-1} q'' = 0–5.99 W cm^{-2} x = 0.03–0.55
Haynes and Fletcher (2003)	R-11, R-123 D_h = 0.92–1.95 mm	G = 110–1840 kg m^{-2} s^{-1} q'' = 1.1–17.0 W cm^{-2} x = 0.0–1.0
Sumith et al. (2003)	Water D_h = 1.45 mm	G = 23.4–152.7 kg m^{-2} s^{-1} q'' = 1–71.5 W cm^{-2} x = 0.0–0.7
Balasubramanian and Kandlikar (2005)	Water, several refrigerants D_h = 0.19–2.92 mm	G = 50–570 kg m^{-2} s^{-1} q'' = 0.5–9.1 W cm^{-2} x = 0.00–0.98
Thome et al. (2004a, 2004b)	R-11, R-12, R-113, R-123, R-134a, R-141b, CO2 D_h = 0.7–3.1 mm	G = 50–502 kg m^{-2} s^{-1} q'' = 0.5–17.8 W cm^{-2} x = 0.01–0.99
Lee and Mudawar (2005)	R-134a, water D_h = 0.35 mm	G = 127–654 kg m^{-2} s^{-1} q'' = 15.9–93.8 W cm^{-2} x = 0.26–0.87
Zhang et al. (2005)	Water, R-11, R-12, and R-113 D_h = 0.78–6.0 mm	G = 23.4–560 kg m^{-2} s^{-1} q'' = 0.3–80.3 W cm^{-2} x = 0.0–0.7
Yun et al. (2006)	R-410A D_h = 1.36, 1.44 mm	G = 200–400 kg m^{-2} s^{-1} q'' = 1–2 W cm^{-2} x = 0.1–0.85
Saitoh et al. (2007)	R-134a D_h = 0.5–11.0 mm	
Cooper (Pool boiling) (1984)	Water, refrigerants, organic fluids, cryogens	q'' = 0.01–60 W cm^{-2}
Gorenflo (Pool boiling) (1993)	Several refrigerants, water and cryogenics	q'' = 0–30 W cm^{-2}

and pressure drop by Harirchian and Garimella (2008) showed that the heat transfer coefficient was largely unaffected by increases in channel width beyond 0.4 mm.

4. Comparison of experiments and predictions

A large number of heat transfer correlations that have been proposed in the literature for predicting the heat transfer coefficient during flow boiling in tubes and channels were collected and discussed in Bertsch et al. (2008b). The predictions from seventeen of these correlations are compared to the measurements from the current work. A majority of the correlations were developed for conventional-sized channels, while some were specifically developed for minichannels and microchannels. In addition to the flow boiling heat transfer correlations, two widely used pool boiling correlations are also included in the comparison. Table 3 provides a summary of the conditions and ranges of applicability of the correlations considered. The correlations are not listed in this paper but are available in Bertsch et al. (2008b). Fluid properties were calculated using EES (Klein, 1992–2007) and the surface tension for R-245fa was correlated with a polynomial fit to data obtained from Refprop7 (2002) with a deviation of less than 0.15% within the operating range, since it was not included in EES.

4.1. Predicted and measured heat transfer coefficient versus vapor quality

Fig. 10 shows the predictions of the heat transfer coefficient from nine of the correlations as a function of vapor quality, together with the corresponding measurement results. Only the widely used correlations and the correlation with the best fit to the data are presented. Flow boiling correlations which are not valid over the whole vapor quality range are only plotted in the appropriate ranges. Four different parameter sets including both channel dimensions were chosen from the experimental results for R-134a. The heat fluxes ranged from 2.5 to 19.6 W cm^{-2} and the mass fluxes ranged from 20 to 334 kg m^{-2} s^{-1}. The saturation pressure was fixed at 550 kPa.

While the Bennett and Chen (1980) correlation captures the absolute value of the heat transfer coefficient at low vapor qualities well, it was designed for conventional-sized channels and shows an increase in heat transfer coefficient with increasing vapor

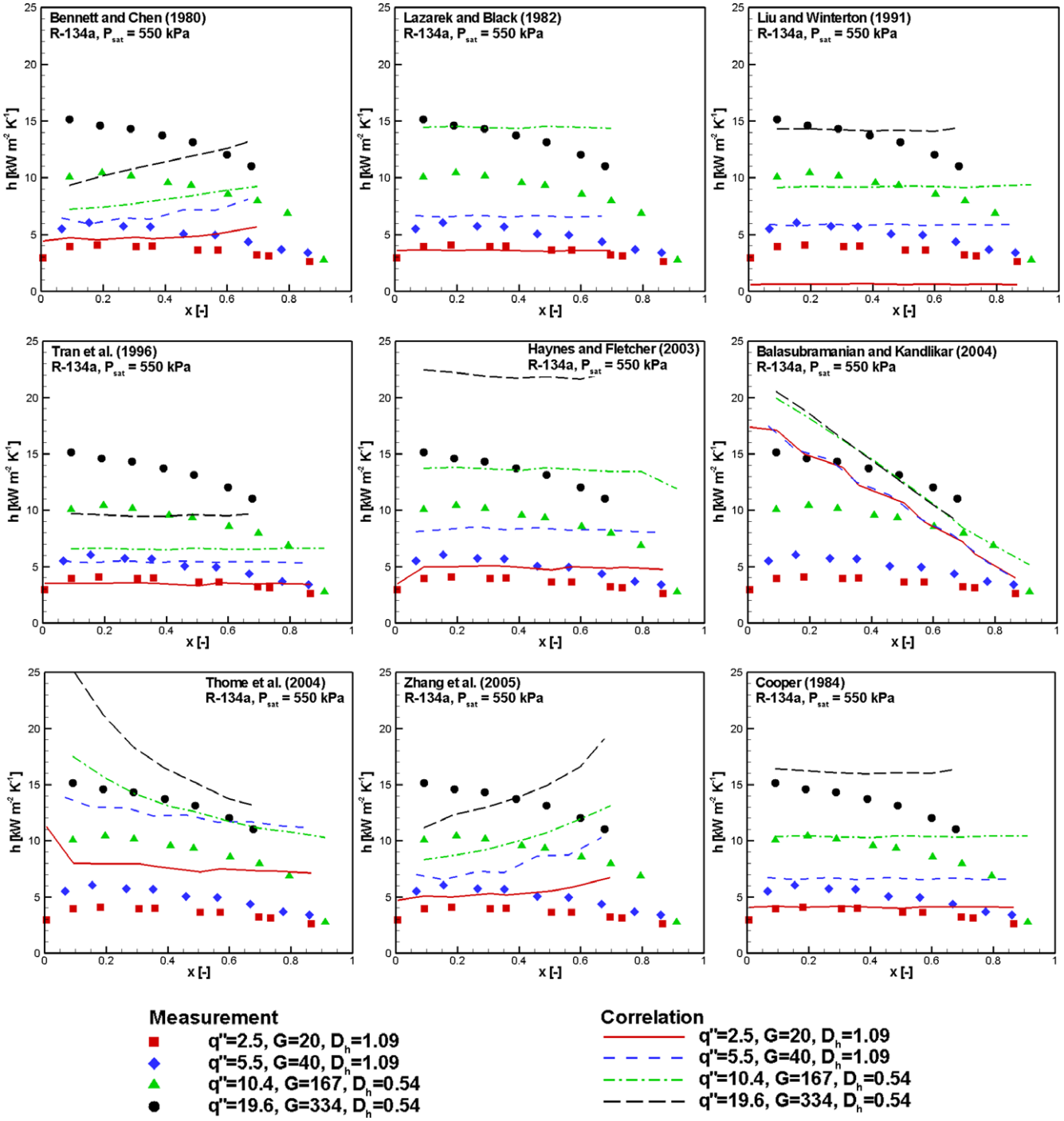

Fig. 10. Comparison between measurements and predictions from several correlations for flow boiling heat transfer for the refrigerant R-134a (G in kg m^{-2} s^{-1}, q'' in W cm^{-2}, D_h in mm).

quality, which deviates from the results in the current study. Similar behavior was found for the Zhang et al. (2005) correlation, which is a modification of the Bennett and Chen (1980) correlation. The heat transfer coefficients calculated by Lazarek and Black (1982), Liu and Winterton (1991), Tran et al. (1996), and Haynes and Fletcher (2003) are all independent of the vapor quality. While the correlation of Liu and Winterton (1991) captures the heat transfer coefficient mainly at high-heat and mass flux, Tran et al. (1996) shows better results at low heat and mass flux. Only the Thome et al. (2004a) correlation and the Balasubramanian and Kandlikar (2005) correlations capture the major trend of heat transfer coefficient as a function of thermodynamic vapor quality. Of these, the physics-based Thome et al. (2004a, 2004b) correlation captures the effects of heat and mass flux better.

4.2. Quantitative assessment of the error values

In addition to the graphical comparison of the predictions obtained with the nine correlations considered in Fig. 10, two characteristic parameters were calculated to provide a quantitative comparison of all correlations listed in Table 3. The absolute error (MAE) was calculated as defined below:

Table 4
Mean absolute error (MAE), and the percentage of predictions which fall within ±30% of the measurement results from each data set[11].

Author(s) of correlation	Mean absolute error (MAE)				Amount of predictions within ±30% of the measurement			
	T.s. #1[(a)] R-134a	T.s. #2[(b)] R-134a	T.s. #2 R-245fa	Average[(c)]	T.s. #1 R-134a	T.s. #2 R-134a	T.s. #2 R-245fa	Average[(d)]
Bennett and Chen (1980)	77.9	56.3	49.9	61.4	46	57.6	50	**51.2**
Bennett et al. (1980)	38.6	25.3	28.8	**30.9**	56.5	68.3	61.4	**62.1**
Lazarek and Black (1982)	54.1	70.5	45.1	56.6	38.9	29.1	38.9	35.6
	38.4	51.7	38.2	42.8	45.7	33.8	45.5	41.6
Shah (1982)	33.4	115.8	208.7	119.3	53.1	22.4	11.1	28.9
	26.3	94.4	176.4	99	57.6	25.9	13.6	32.4
Liu and Winterton (1991)	50.2	26.6	21.2	**32.7**	42.5	75.8	79.6	**66**
	39.4	15.2	17.5	**24.1**	52.2	86.3	86.4	**75**
Tran et al. (1996)	26.8	35	40.5	**34.1**	73.5	38.8	18.5	43.6
	16.6	33.3	44.7	**31.6**	89.1	33.8	6.8	43.3
Lee and Lee (2001)	102	210.1	292.5	201.6	29.2	7.9	0	12.4
	66.7	122	200.7	129.8	35.9	9.4	0	15.1
Warrier et al. (2002)	76.5	60.2	64.5	67.1	33.6	38.8	46.3	39.6
	50.9	37.4	38.7	42.3	41.3	44.6	56.8	47.6
Haynes and Fletcher (2003)	84.6	58	46.9	63.2	9.7	30.3	42.6	27.5
	66.9	42.1	38.9	49.3	12	36	50	32.6
Sumith et al. (2003)	51.4	44.5	30.3	42.1	15	35.2	64.8	38.3
	53.5	40.2	24.7	39.5	12	33.8	65.9	37.2
Balasubramanian and Kandlikar (2005)	119.6	81.4	72.4	91.1	10.6	33.3	16.7	20.2
	137.4	82.8	70.4	96.9	4.3	32.4	18.2	18.3
Thome (2004)	161	51.4	23.1	78.5	0	34.5	75.9	36.8
	139.8	37.3	24.6	67.3	0	38.8	70.5	36.4
Lee and Mudawar (2005)	44.6	54.2	60.2	53	38.9	41.2	38.9	39.7
	40.5	55.9	62	52.8	47.8	42.4	43.2	44.5
Zhang et al. (2005)	127.9	99.5	81.4	103	31.9	57	48.1	45.7
	65.9	32	36.3	44.7	39.1	67.6	59.1	**55.3**
Yun et al. (2006)	269.4	182.2	282.3	244.6	0	0	0	0
	217.2	119.3	220.8	185.7	0	0	0	0
Saitoh et al. (2007)	65	51.9	57.9	58.3	25.7	43.6	35.2	34.8
	48	34.6	46.6	43.1	31.5	51.1	40.9	41.2
Cooper (1984)	47.5	31.6	24.6	**34.6**	46.9	70.3	70.4	**62.5**
	32.5	17.2	19.1	**22.9**	57.6	81.3	79.5	**72.8**
Gorenflo et al. (1993)	88.1	62.8	51.7	67.5	10.6	30.3	33.3	24.8
	68.5	43.3	42	51.3	13	36	38.6	29.2

[(a)] Test section #1: D_h = 1.09 mm, n = 17.
[(b)] Test section #2: D_h = 0.54 mm, n = 33.
[(c)] Error values below 40% highlighted.
[(d)] Values above 50% highlighted.

$$\mathrm{MAE} = \frac{1}{N}\sum_{N}\frac{\|h_{\mathrm{calc}} - h_{\mathrm{meas}}\|}{h_{\mathrm{meas}}} \tag{10}$$

In addition, the number of predicted heat transfer coefficients that fall within ±30% of the measured data is determined. These two measures of the goodness of the comparisons are presented in Table 4 for all the correlations considered with respect to the three different experimental data sets – measurements with R-134a on test sections #1 and #2, and with R-245fa on test section #2. Table 4 also lists the average error values.

The two characteristic values were calculated twice; once for the complete data sets, and then a second time for vapor qualities below 0.7 only. This measure ensured a fair comparison that avoided the extrapolation of some of the correlations that are restricted to a lower vapor quality range.

The average was calculated by database and not based on the number of data points in each database in order to avoid skewing the comparison due to different-sized data sets. Mean absolute error (MAE) values of less than 40% are highlighted in bold font for ease of identification. In addition, if more than half of the data points were predicted to within ±30%, the mean values are highlighted in bold font as well.

The overall best prediction – identified as that which provides the lowest MAE and the largest percentage of data predicted to within ±30% of the measurements – is the Liu and Winterton (1991) correlation closely followed by the pool boiling equation of Cooper (1984). The Bennett and Chen (1980) correlation also works reasonably well when restricted to vapor qualities below 0.7. The success of this pool boiling correlation in predicting the present results again points to a dominance of nucleate boiling over convective boiling. It should be noted that Liu and Winterton (1991) correlation is a superposition approach of convective heat transfer and nucleate boiling using the Cooper (1984) correlation.

In summary, even those correlations identified in this relative assessment as the best ones do not provide accurate predictions. Correlations that have been developed specifically for minichannels and microchannels show no essential improvement over those developed earlier for conventional-sized channels. Not surprisingly, correlations that were proposed based on a curvefit to a single data set do not extrapolate well beyond the very narrow parameter ranges of the tests. Therefore, additional research into the mechanisms of flow boiling in small channels is necessary, so that accurate flow boiling equations may be proposed. Models based on the physics of the boiling process and the appropriate flow patterns and regime maps are likely to yield better to extrapolation beyond the boundaries of the operating ranges relative to purely empirical correlations.

5. Conclusions

An experimental study was carried out to investigate the heat transfer coefficient during refrigerant flow boiling in two microchannel heat exchangers with channel hydraulic diameters of

1.09 and 0.54 mm. All boundary conditions are well specified and a verification of the energy balance in the setup produced excellent and repeatable results. The major conclusions of the study are:

- The heat transfer coefficient for R-245fa in comparison with R-134a in single-phase flow is higher. On the other hand, the pool boiling heat transfer for R-245fa is lower as a result of its higher molecular mass and surface tension. This results in superior heat transfer for R-134a in the flow boiling regime.
- The onset of nucleate boiling (ONB) is shifted towards higher heat fluxes with increasing mass flux for both fluids in the investigated parameter range.
- The flow boiling heat transfer coefficient strongly increases with increasing heat flux and seems to be dominated by nucleate boiling. It also shows a strong dependence on thermodynamic vapor quality with a rapid decrease at qualities above 0.5. The maximum heat transfer coefficient occurs at vapor qualities between 0.1 and 0.5 depending on fluid, geometry and flow conditions. The heat transfer coefficient increases weakly with increasing mass flux and is almost constant for the range of saturation temperatures investigated in this study. The smaller hydraulic diameter leads to marginally higher heat transfer coefficients.
- A comparison of the measurements against predictions from several correlations in the literature showed reasonable agreement only with a very few correlations. Among the correlations which delivered the lowest errors were a pool boiling equation (Cooper, 1984) and two flow boiling equations which were developed for conventional-sized channels (Liu and Winterton, 1991; Tran et al. 1996). Equations that were developed specifically for small channels did not predict the heat transfer coefficient better.

Acknowledgement

The authors acknowledge the financial support from members of the Cooling Technologies Research Center, a National Science Foundation Industry/University Cooperative Research Center at Purdue University.

References

Balasubramanian, P., Kandlikar, S.G., 2005. Experimental study of flow patterns, pressure drop, and flow instabilities in parallel rectangular minichannels. Heat Transfer Eng. 26, 20–27.
Bao, Z.Y., Fletcher, D.F., Haynes, B.S., 2000. Flow boiling heat transfer of Freon R11 and HCFC123 in narrow passages. Int. J. Heat Mass Transfer 43, 3347–3358.
Bennett, D.L., Chen, J.C., 1980. Forced convective boiling in vertical tubes for saturated pure components and binary mixtures. AIChE J. 26, 454–461.
Bennett, D.L., Davies, M.W., Hertzler, B.L., 1980. The Suppression of Saturated Nucleate Boiling by Forced Convective Flow, American Institute of Chemical Engineers Symposium Series, vol. 76, pp. 91–103.
Bertsch, S.S., Groll, E.A., Garimella, S.V., 2008a. Refrigerant flow boiling heat transfer in parallel microchannels as a function of local vapor quality. Int. J. Heat Mass Transfer 51, 4775–4787.
Bertsch, S.S., Groll, E.A., Garimella, S.V., 2008b. Review and comparative analysis of studies on saturated flow boiling in small channels. Nanoscale Microscale Thermophys. Eng. 12, 187–227.
Calm, J.M., Hourahan, G.C., 2001. Refrigerant data summary. Eng. Sys. 18, 74–88.
Chang, K.H., Pan, C., 2007. Two-phase flow instability for boiling in a microchannel heat sink. Int. J. Heat Mass Transfer 50, 2078–2088.
Chen, T., Garimella, S.V., 2006. Measurements and high-speed visualizations of flow boiling of a dielectric fluid in a silicon microchannel heat sink. Int. J. Multiphase Flow 32, 957–971.
Cooper, M.G., 1984. Heat flow rates in saturated nucleate pool boiling – A wide-ranging examination using reduced properties. Adv. Heat Transfer 16, 157–239.
Dupont, V., Thome, J.R., 2005. Evaporation in microchannels: influence of the channel diameter on heat transfer. Microfluidics Nanofluidics 1, 119–127.
Garimella, S.V., Sobhan, C.B., 2003. Transport in microchannels – a critical review. Ann. Rev. Heat Transfer 13, 1–50.
Garimella, S.V., Singhal, V., Liu, D., 2006. On-chip thermal management with microchannel heat sinks and integrated micropumps. Proc. IEEE 94, 1534–1548.
Gorenflo, D., 1993, Pool boiling, VDI Heat Atlas, Verein Deutscher Ingenieure, VDI-Gesellschaft Verfahrenstechnik und Chemieingenieurwesen, ISBN-3184009157.
Haynes, B.S., Fletcher, D.F., 2003. Subcooled flow boiling heat transfer in narrow passages. Int. J. Heat Mass Transfer 46, 3673–3682.
Harirchian, T., Garimella, S.V., 2008. Microchannel size effects on local flow boiling heat transfer to a dielectric fluid. Int. J. Heat Mass Transfer 51, 3724–3735.
Hausen, H., 1943. Darstellung des Wärmeüberganges in Rohren durch verallgemeinerte Potenzbeziehungen. Z. VDI Beiheft Verfahrenstechnik 4, 91–102.
Hetsroni, G., Klein, D., Mosyak, A., Segal, Z., Pogrebnyak, E., 2004. Convective boiling in parallel microchannels. Microscale Thermophys. Eng. 8, 403–421.
Kandlikar, S.G., Steinke, M.E., 2003, Predicting heat transfer during flow boiling in minichannels and microchannels, ASHRAE Trans. 109 (1), CH-03-13-1.
Kedzierski, M.A., 2006. A comparison of R245fa pool boiling measurements to R123, and R245fa/Isopentane on a passively enhanced, horizontal surface. Int. J. Transport Phenomena 8, 331–344.
Klein, S.A., 1992–2007, Engineering Equation Solver, F-Chart Software, www.fChart.com.
Lazarek, G.M., Black, S.H., 1982. Evaporative heat transfer, pressure drop and critical heat flux in a small vertical tube with R-113. Int. J. Heat Mass Transfer 25, 945–960.
Lee, J., Mudawar, I., 2005. Two-phase flow in high-heat flux micro-channel heat sink for refrigeration cooling applications: Part II–heat transfer characteristics. Int. J. Heat Mass Transfer 48, 941–955.
Lee, P.S., Garimella, S.V., 2007. Saturated flow boiling heat transfer and pressure drop in silicon microchannel arrays. Int. J. Heat Mass Transfer 51, 789–806.
Lee, P.S., Garimella, S.V., Liu, D., 2005. Investigation of heat transfer in rectangular microchannels. Int. J. Heat Mass Transfer 48, 1688–1704.
Lee, H.J., Lee, S.Y., 2001. Heat transfer correlation for boiling flows in small rectangular horizontal channels with low aspect ratios. Int. J. Multiphase Flow 27, 2043–2062.
Lin, S., Kew, P.A., Cornwell, K., 2001. Two-phase heat transfer to a refrigerant in a 1 mm diameter tube. Int. J. Refrig. 24, 51–56.
Liu, D., Lee, P., Garimella, S.V., 2005. Prediction of the onset of nucleate boiling in microchannel flow. Int. J. Heat Mass Transfer 48, 5134–5149.
Liu, Z., Winterton, R.H.S., 1991. A general correlation for saturated and subcooled flow boiling in tubes and annuli, based on a nucleate pool boiling equation. Int. J. Heat Mass Transfer 34, 2759–2766.
Mongia, R., Masahiro, K., DiStefano, E., 2006, Small scale refrigeration system for electronics cooling within a notebook computer, Proc. ITHERM'06.
Qu, W., Mudawar, I., 2004. Transport phenomena in two-phase micro-channel heat sinks. J. Electron. Pack. 126, 213–224.
Refprop7, 2002, Reference Fluid Thermodynamic and Transport Properties, NIST Standard Reference Database 23, Version 7.0.
Revellin, R., Thome, J.R., 2007. Experimental investigation of R-134a and R-245fa two-phase flow in microchannels for different flow conditions. Int. J. Heat Fluid Flow 28, 63–71.
Saitoh, S., Daiguji, H., Hihara, E., 2007. Correlation for boiling heat transfer of R-134a in horizontal tubes including effect of tube diameter. Int. J. Heat Mass Transfer 50, 5215–5225.
Saitoh, S., Daiguji, H., Hihara, E., 2005. Effect of tube diameter on boiling heat transfer of R-134a in horizontal small-diameter tubes. Int. J. Heat Mass Transfer 48, 4473–4984.
Sieder, E.N., Tate, G.E., 1936. Heat transfer and pressure drop of liquids in tubes. Ind. Eng. Chem. 28, 1428–1436.
Shah, M.M., 1982. Chart correlation for saturated boiling heat transfer: equations and further study. ASHRAE Trans. 88, 185–196.
Sobhan, C.B., Garimella, S.V., 2001. A comparative analysis of studies on heat transfer and fluid flow in microchannels. Microscale Thermophys. Eng. 5, 293–311.
Steinke, M.E., Kandlikar, S.G., 2004. An experimental investigation of flow boiling characteristics of water in parallel microchannels. Trans. ASME 126, 518–526.
Sumith, B., Kaminaga, F., Matsumura, K., 2003. Saturated flow boiling of water in a vertical small diameter tube. Exp. Thermal Fluid Sci. 27, 789–801.
Tadrist, L., 2007. Review on two-phase flow instabilities in narrow spaces. Int. J. Heat Fluid Flow 28, 54–62.
Taylor, J.R., 1997. An Introduction to Error Analysis, second ed. University Science Books.
Thome, J.R., 2004. Boiling in microchannels: a review of experiment and theory. Int. J. Heat Fluid Flow 25, 128–139.
Thome, J.R., Dupont, V., Jacobi, A.M., 2004a. Heat transfer model for evaporation in microchannels. Part I: presentation of the model. Int. J. Heat Mass Transfer 47, 3375–3385.
Thome, J.R., Dupont, V., Jacobi, A.M., 2004b. Heat transfer model for evaporation in microchannels. Part II: comparison with the database. Int. J. Heat Mass Transfer 47, 3387–3401.
Tran, T.N., Wambsganss, M.W., France, D.M., 1996. Small circular and rectangular-channel boiling with two refrigerants. Int. J. Multiphase Flow 22, 485–498.
Trutassanawin, S., Groll, E.A., Garimella, S.V., Cremaschi, L., 2006. Experimental investigation of a miniature-scale refrigeration system for electronics cooling. IEEE Trans. Compon. Pack. Technol. 29, 678–687.

Vlasie, C., Macchi, H., Guilpart, J., Agostini, B., 2004. Flow boiling in small diameter channels. Int. J. Refrig. 27, 191–201.

Warrier, G.R., Dhir, V.K., Momoda, L.A., 2002. Heat transfer and pressure drop in narrow rectangular channels. Exp. Thermal Fluid Sci. 26, 53–64.

Wu, H.Y., Cheng, P., 2003. Visualization and measurements of periodic boiling in silicon microchannels. Int. J. Heat Mass Transfer 14, 2603–2614.

Yan, Y., Lin, T., 1998. Evaporation heat transfer and pressure drop of refrigerant R-134a in a small pipe. Int. J. Heat Mass Transfer 41, 4183–4194.

Yun, R., Heo, J.H., Kim, Y., 2006. Evaporative heat transfer and pressure drop of R410A in microchannels. Int. J. Refrig. 29, 92–100.

Zhang, W., Hibiki, T., Mishima, K., 2005. Correlation for flow boiling heat transfer at low liquid Reynolds number in small diameter channels. J. Heat Transfer 127, 1214–1221.